Available online at www.sciencedirect.com
ScienceDirect
Polymer 48 (2007) 6519–6531
polymer
www.elsevier.com/locate/polymer

Rate and molecular weight distribution modeling of syndiospecific styrene polymerization over silica-supported metallocene catalyst

Joong Jin Han [a], Hyung Woo Lee [a,1], Won Jung Yoon [b], Kyu Yong Choi [a,*]

[a] Department of Chemical and Biomolecular Engineering, University of Maryland, Building 090, College Park, MD 20742, USA
[b] Department of Chemical Bioengineering, Kyungwon University, San 65 Bokjeong-dong, Sujeong-gu, Seongnam, Gyeonggi-do, Korea

Received 16 July 2007; received in revised form 30 August 2007; accepted 2 September 2007
Available online 7 September 2007

Abstract

The kinetics of syndiospecific polymerization of styrene over silica-supported Cp*Ti$(OCH_3)_3$/MAO catalyst has been investigated through experimentation and theoretical modeling. At low monomer concentrations, the polymerization rate increases almost linearly with monomer conversion, but the reaction rate becomes independent of monomer concentration at high bulk phase monomer concentrations. A kinetic model that incorporates the monomer partition effect between the solid and the liquid phases has been proposed. The model simulations show that the observed non-linear kinetics can be adequately modeled by the monomer partition model. The polymer molecular weight has also been found to increase with the monomer concentration and the polymer molecular weight distribution (MWD) is quite broad, suggesting that the catalytic behavior deviates from the single site catalytic polymerization model. The MWD broadening is modeled by a two-site kinetic model and a good agreement between the model and the experimental data has been obtained.

Keywords: Syndiotactic polystyrene; Metallocene catalyst; Polymerization kinetics

1. Introduction

Syndiotactic polystyrene (sPS) is a semicrystalline thermoplastic polymer with many advantageous properties. For example, sPS has excellent heat resistance with a melting point of 270 °C, strong chemical resistance against acids, bases, oils and water, and low dielectric constant [1]. The catalytic synthesis of sPS has been investigated by many researchers since Ishihara et al. [2,3], and a review by Schellenberg and Tomotsu [4] provides a comprehensive overview of the recent developments of metallocene catalyst systems for the syndiospecific polymerization of styrene.

The polymerization of sPS with either homogeneous or heterogeneous metallocene catalyst is characterized by the precipitation of sPS because sPS does not dissolve in its own monomer (styrene) and organic solvents at typical reaction temperatures (e.g., <100 °C). In sPS polymerization over a homogeneous (or soluble) metallocene catalyst, polymer microparticles agglomerate as monomer conversion increases and these sPS agglomerates become a gel that is a wet cake-like material. With further increase in monomer conversion, the gel becomes hard. The sPS gel is not a chemically cross-linked gel but a physical gel. It is believed that strong intermolecular interactions between the polymer and the monomer/solvent molecules are the main cause for the gelation. Once sPS gel is formed, the reaction mixture becomes extremely difficult to agitate by conventional means. Therefore, developing a polymerization process that can avoid the gelation is of important industrial interest.

Abbreviations: MAO, methyl aluminoxane; MMAO, modified methyl aluminoxane; MEK, methyl ethyl ketone; MWD, molecular weight distribution; PVC, poly(vinyl chloride); sPS, syndiotactic polystyrene; TSC, total solid content.

* Corresponding author. Tel.: +1 301 405 1907; fax: +1 301 405 0523.
E-mail address: choi@umd.edu (K.Y. Choi).
[1] Present address: Pt. Garuda Twin Jaya, JL. Teuku Nyak Arief #10, Jakarta 12220, Indonesia.

0032-3861/$ - see front matter © 2007 Elsevier Ltd. All rights reserved.
doi:10.1016/j.polymer.2007.09.006

Nomenclature

[Al]	aluminum concentration [mol/L]
C_0	initial potent catalyst site [−]
C*	activated catalyst site [−]
$[C^*]_0$	initial catalyst concentration [mol/L]
D*	deactivated catalyst site [−]
f_L	volume fraction of liquid phase [−]
k_d	catalyst deactivation rate constant [1/h]
k_p	propagation rate constant [L/mol h]
k_{tM}	chain transfer to monomer rate constant [L/mol h]
$k_{t\beta}$	β-hydrogen elimination rate constant [1/h]
K_1, K_2	partition coefficients of monomer between liquid and solid phases [−], [L/mol]
M	monomer [−]
$[M]_{b0}$	initial monomer concentration [mol/L]
M_n	dead polymer chain of length n [−]
$\overline{M}_n$	number-average molecular weight [g/mol]
$[M]_s$	monomer concentration in the solid phase [mol/L]
$\overline{M}_w$	weight-average molecular weight [g/mol]
$(mw)_{sty}$	molecular weight of styrene [g/mol]
[P]	total live polymer concentration [mol/L]
P_n	live polymer chain of length n [−]
R_d	catalyst deactivation rate [mol/L h]
R_p	polymerization (propagation) rate [mol/L h]
R_t	chain transfer rates [mol/L h]
[Ti]	catalyst (titanium) concentration [mol Ti/L]
V_L	liquid phase volume [L]
V_S	solid phase volume [L]
V_{slurry}	total slurry volume [L]
W_D	weight of diluent (heptane) [g]
$W_i(x)$	weight fraction of the polymer of chain length x produced by the active site i [−]
W_M	weight of monomer [g]
W_{sPS}	weight of sPS [g]
$\overline{X}_n$	number-average degree of polymerization [−]
X_w	weight chain length distribution [−]

Greek letters

ϕ_i	weight fraction of active site i [−]
Φ	amount of liquid absorbed in 1 g of sPS polymer [L/g sPS]
λ_{Pk}	kth moment of live polymers [−]
λ_{Mk}	kth moment of dead polymers [−]
ρ_D	density of diluent [g/L]
ρ_M	density of monomer [g/L]
ρ_{sPS}	density of sPS [g/L]

Although the synthesis of sPS has been investigated with various types of metallocene catalysts, little has been reported on the quantitative analysis of sPS polymerization kinetics [5–8]. Also, very little is known about the phase transition of a polymerization mixture in either homogeneously or heterogeneously catalyzed styrene polymerization.

In our previous work, we reported the kinetics of styrene polymerization over homogeneous and heterogenized $Cp^*Ti(OCH_3)_3$/MAO catalysts [8–10]. When a liquid slurry polymerization process is employed with heterogeneous catalysts, sPS can be recovered as discrete particles. One of the simple techniques to heterogenize a homogeneous metallocene catalyst is the catalyst embedding technique where active titanium–MAO complex is embedded into a homogeneous mass of sPS prepolymer [8,9]. The sPS polymerization with the embedded catalyst showed that there was a range of polymerization conditions that allowed for the formation of sPS particles without significant particle agglomeration or gelation [9,10].

In this paper, we present our new experimental and mathematical modeling study of a slurry phase sPS polymerization over silica-supported metallocene catalyst.

2. Experimental

2.1. Materials

Styrene (Aldrich) was vacuum distilled over calcium hydride and activated alumina was used to remove inhibitor from the monomer. *n*-Heptane (Fisher Scientific) was used as a diluent and it was purified by being refluxed over sodium and benzophenone in nitrogen atmosphere. $Cp^*Ti(OCH_3)_3$ (pentamethyl cyclopentadienyl titanium trimethoxide) (Strem Chemicals) and modified methyl aluminoxane (MMAO, Akzo Nobel) were used as-supplied without further purification. Silica gel (Davison 952, W.R. Grace) was used as a catalyst support.

2.2. Preparation of supported catalysts

Silica gel was calcined at 250 °C for 24 h under nitrogen atmosphere. The calcined silica gel was then treated with an MMAO solution (1.6 mmol of MMAO and 20 mL of toluene per 1 g of silica gel, mixed at 50 °C for 1.5 h), washed with toluene, and dried in vacuo. Then, the silica support was mixed with a $Cp^*Ti(OCH_3)_3$ catalyst solution (0.5 mmol of $Cp^*Ti(OCH_3)_3$ and 35 mL of toluene per 1 g of MMAO–silica, mixed at 50 °C for 1 h), washed with toluene, and dried in vacuo for 24 h. The Al and Ti loadings measured by inductively coupled plasma emission spectroscopy (ICP) were 1.30×10^{-3} mol Al/g catalyst and 2.92×10^{-4} mol Ti/g catalyst, respectively.

2.3. Slurry phase styrene polymerization

Slurry phase styrene polymerization experiments were carried out using an 100 mL jacketed glass reactor equipped with a stainless steel agitator. Predetermined amounts of monomer, solvent, catalyst, and MMAO were charged into the reactor in a glove box. All the polymerization experiments were carried out at 70 °C and the agitator speed was maintained constant during the polymerization. The initial catalyst concentration was fixed at 2.62×10^{-4} mol Ti/L and the Al/Ti mole ratio

was fixed at 500. After polymerization, the reaction mixture was removed from the reactor, washed with excess amount of acidified methanol (10 vol.% of hydrochloric acid), and dried in vacuo. Since the reactor has no provisions for sampling during the polymerization, the polymer yield vs. time profiles were obtained by conducting the individual experiments with same reaction conditions but terminated at different reaction times. The monomer conversion was determined gravimetrically by measuring the polymer weight for a known amount of initial monomer and diluent. The total solid content (TSC) was determined by measuring the weight of the initial reaction mixture and the weight of the polymer produced (i.e., TSC = polymer weight/initial weight of reaction mixture). The methyl ethyl ketone (MEK) insoluble fraction was used as a quick but approximate measure of the syndiotacticity. Most of the sPS samples showed that the MEK insoluble fractions were in the range of 93–95%. The number- and weight-average molecular weights were determined by gel permeation chromatography (GPC) with 1,2,3-trichlorobenzene at 135 °C using PLgel® 10 μm MIXED-B and PLgel® 10 μm GUARD columns (Polymer Laboratories).

3. Experimental results and discussion

3.1. Polymerization rate analysis

We carried out styrene polymerization experiments at different monomer and catalyst concentrations. The same batch of catalyst was used in all these experiments to minimize the run-to-run variations in catalyst activity. Table 1 shows a summary of experimental results of 20 polymerization runs at 70 °C. We use the same amount of catalyst and Al/Ti mole ratio in all these experiments.

In our first series of polymerization experiments, we investigated the effect of bulk phase monomer concentration on the polymer yield and polymerization rate. Fig. 1(a) and (b) shows the polymer yield and polymerization rate data (symbols) obtained for four different initial styrene concentrations ($[M]_{b0}$). For each polymerization experiment, the polymerization rate values were determined by numerically differentiating a polymer yield vs. time curve with ORIGIN® package (OriginLab, Ver. 7.5). Since the polymerization was carried out in a batch reactor, the decrease in the polymerization rate was due to the consumption of monomer as well as the catalyst deactivation. The polymer yield data shown in Fig. 1(a) indicate that the polymer yield does not increase linearly in proportion to the initial monomer concentration. This observation suggests that the sPS polymerization rate deviates from the first-order kinetics with respect to monomer concentration.

To determine the dependence of polymerization rate on the monomer concentration, initial polymerization rates are plotted against initial monomer concentrations as shown in Fig. 2. The initial polymerization rate values were estimated by extrapolating the polymerization rate data to $t = 0$. It is observed that the initial polymerization rate increases almost linearly in proportion to monomer concentration up to about 2.0 mol/L. At monomer concentrations higher than

Table 1
Reaction conditions and experimental data of sPS polymerization with silica-supported metallocene catalyst

Run ID [−]	$[M]_{b0}$ [mol/L]	$[Ti] \times 10^4$ [mol/L]	St [vol.%]	Reaction time [min]	Yield [g]	TSC [w/w%]	Avg. activity $\times 10^{-3}$ [g sPS/mol Ti min]	$M_w \times 10^{-5}$ [g/mol]	PDI [−]
1-1	0.81	2.62	10	10	1.45	4.9	8.58	1.32	4.10
1-2				30	2.34	6.9	4.62		
1-3				60	2.69	7.7	2.65		
1-4				120	2.97	8.2	1.46		
2-1	2.02	2.62	25	10	3.08	8.1	18.22	1.70	3.06
2-2				30	4.64	11.3	9.15		
2-3				60	5.96	14.1	5.88		
2-4				120	7.81	17.9	3.85		
3-1	3.24	2.62	40	10	3.49	8.6	20.65	2.65	3.74
3-2				30	5.30	12.2	10.45	2.42	3.04
3-3				60	7.92	17.4	7.81	2.21	3.24
3-4				120	12.14	27.8	5.99	2.39	3.71
4-1	4.86	2.62	60	10	3.11	7.4	18.40	3.15	3.44
4-2				30	6.59	14.0	13.00		
4-3				60	10.13	20.7	9.99		
4-4				120	13.66	27.4	6.74		
C-1	2.03	0.35	25	15	0.01	0.0	0.31		
C-2		0.70			0.34	0.6	5.35		
C-3		1.37			1.31	2.2	10.34		
C-4		2.68			4.28	7.1	16.88		
C-5		3.92			6.83	11.4	17.93		

Styrene (60 mL) and *n*-heptane was used.
[Al]/[Ti] = 500 (1-1 to 4-4), [Al]/[Ti] = 350 (C-1–C-5).

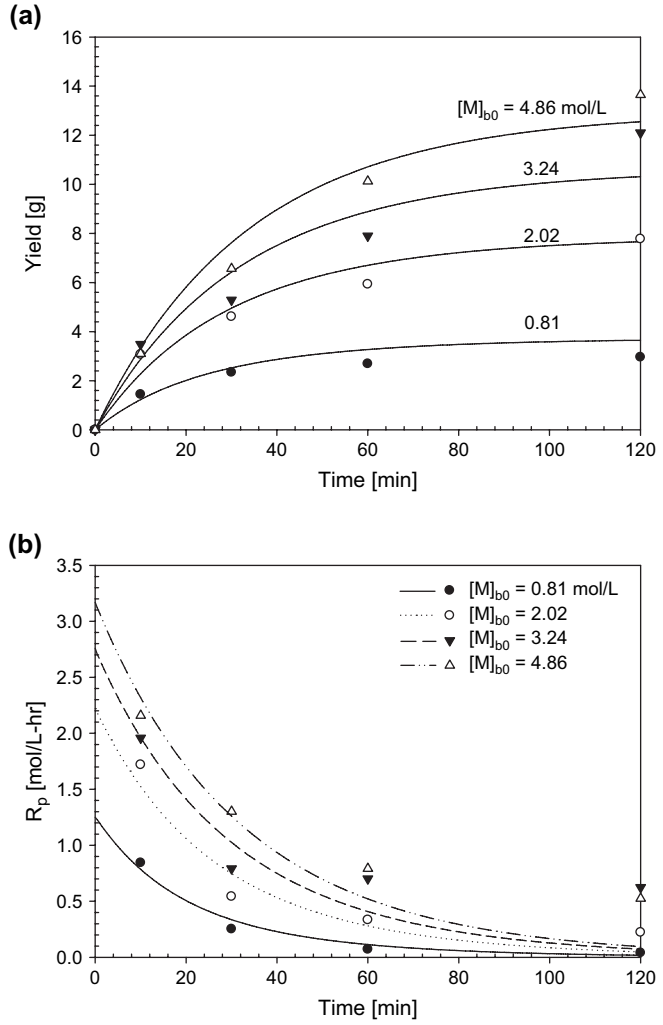

Fig. 1. Effect of initial monomer concentration on polymer yield and polymerization rate at 70 °C (symbols – data (●, 0.81 mol/L; ○, 2.02 mol/L; ▼, 3.24 mol/L; △, 4.86 mol/L), lines – model).

2.0 mol/L, polymerization rate is little dependent on the monomer concentration. The data show that the initial polymerization rate tends to level off for the initial monomer concentrations higher than 2.0 mol/L. Since catalyst deactivation effect can be assumed negligible at the beginning of polymerization, the results shown in Fig. 2 suggest that some other effects might have influenced the polymerization rate. Similar phenomena were observed in styrene polymerization with other heterogeneous catalyst systems (e.g., embedded catalysts [10]). We shall discuss the kinetic analysis of the observed rate phenomena later in this paper.

The effect of catalyst concentration on the initial polymerization has also been investigated and the results are shown in Fig. 3. At very low catalyst concentrations (e.g., $\leq 0.5 \times 10^{-4}$ mol/L), very little amount of polymer was produced. It is probably because at such low catalyst concentrations, the catalyst might have been deactivated by the impurities present in the liquid phase with very little sites left available for polymerization. Over the range of catalyst concentration we tested (i.e., $[\mathrm{Ti}] \geq 0.5 \times 10^{-4}$ mol/L), the sPS polymerization rate shows the first-order dependence on the initial catalyst concentration.

To further analyze the polymerization rate behaviors observed in our experiments, we consider the following reaction kinetic model [9,11].

Catalyst site activation:

$$\mathrm{C}_0 + \mathrm{MAO} \xrightarrow{k_a} \mathrm{C}^* \tag{1}$$

Propagation:

$$\mathrm{C}^* + \mathrm{M} \xrightarrow{k_p} \mathrm{P}_1 \qquad \mathrm{P}_n + \mathrm{M} \xrightarrow{k_p} \mathrm{P}_{n+1} \tag{2}$$

Chain transfer to monomer:

$$\mathrm{P}_n + \mathrm{M} \xrightarrow{k_{t\mathrm{M}}} \mathrm{M}_n + \mathrm{P}_1 \tag{3}$$

β-hydrogen elimination:

$$\mathrm{P}_n \xrightarrow{k_{t\beta}} \mathrm{M}_n + \mathrm{C}^* \tag{4}$$

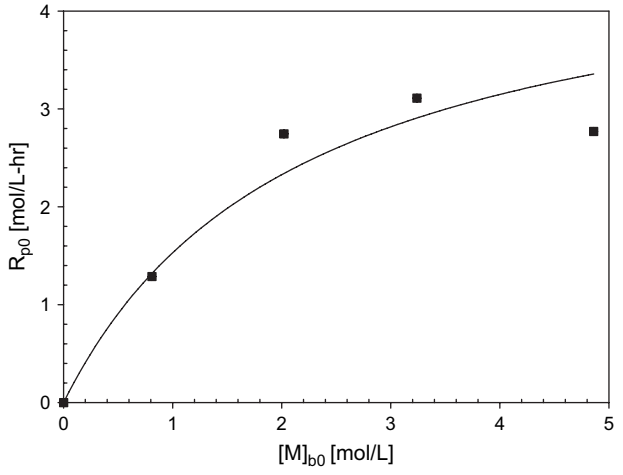

Fig. 2. Initial polymerization rate vs. initial monomer concentration (■ – data; dashed line – model calculations from Eq. (20)).

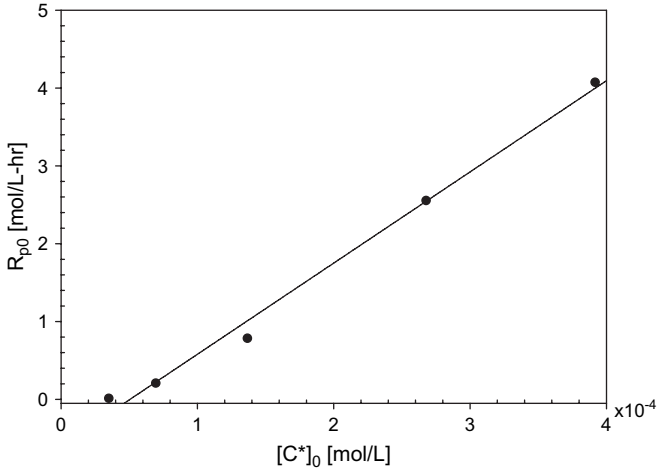

Fig. 3. Polymerization rate vs. initial catalyst concentration ($[\mathrm{M}]_{b0} = 2.03$ mol/L, reaction time = 15 min, $T = 70$ °C, Al/Ti = 350).

Catalyst deactivation:

$$C^* \xrightarrow{k_d} D^* \qquad P_n \xrightarrow{k_d} M_n + D^* \tag{5}$$

where C_0 is the potent catalyst site, C* is the activated catalyst site, P_n and M_n are the live and dead polymer chains of length n, M is the monomer, and D* is the deactivated catalyst site. k_j represents the reaction rate constant for each corresponding reaction. We assume that catalyst activation reaction (Eq. (1)) is very fast. To calculate the molecular weight averages, polymer molecular weight moment equations are needed. The polymerization rate equations and the polymer molecular moment equations are derived as follows:

$$\frac{d[C^*]}{dt} = -k_d[C^*] - k_p[C^*][M]_s + k_{t\beta}\lambda_{P0} \tag{6}$$

$$\frac{d[M]_s}{dt} = -k_p[P][M]_s - k_{tM}[P][M] \approx -k_p[P][M]_s \tag{7}$$

$$\frac{d[P_1]}{dt} = k_p[C^*][M]_s - k_p[P_1][M]_s - k_{tM}[P_1][M]_s + k_{tM}\lambda_{P0}[M]_s - k_{t\beta}[P_1] - k_d[P_1] \tag{8}$$

$$\frac{d[P_n]}{dt} = k_p([P_{n-1}] - [P_n])[M]_s - k_{tM}[P_n][M]_s - k_{t\beta}[P_n] - k_d[P_n] \quad n \geq 2 \tag{9}$$

$$\frac{d[M_n]}{dt} = k_d[P_n] + k_{t\beta}[P_n] + k_{tM}[P_n][M]_s \quad n \geq 2 \tag{10}$$

$$\frac{d\lambda_{P0}}{dt} = k_p[C^*][M]_s - k_{t\beta}\lambda_{P0} - k_d\lambda_{P0} \tag{11}$$

$$\frac{d\lambda_{M0}}{dt} = k_{t\beta}\lambda_{P0} + k_d\lambda_{P0} + k_{tM}\lambda_{P0}[M]_s \tag{12}$$

$$\frac{d\lambda_{P1}}{dt} = k_p[C^*][M]_s + k_p\lambda_{P0}[M]_s + k_{tM}[M]_s(\lambda_{P0} - \lambda_{P1}) - k_{t\beta}\lambda_{P1} - k_d\lambda_{P1} \tag{13}$$

$$\frac{d\lambda_{M1}}{dt} = k_{t\beta}\lambda_{P1} + k_{tM}\lambda_{P1}[M]_s + k_d\lambda_{P1} \tag{14}$$

$$\frac{d\lambda_{P2}}{dt} = k_p[C^*][M]_s + k_p[M]_s(2\lambda_{P1} + \lambda_{P0}) - k_{t\beta}\lambda_{P2} + k_{tM}[M]_s(\lambda_{P0} - \lambda_{P2}) - k_d\lambda_{P2} \tag{15}$$

$$\frac{d\lambda_{M2}}{dt} = k_{t\beta}\lambda_{P2} + k_{tM}\lambda_{P2}[M]_s + k_d\lambda_{P2} \tag{16}$$

where the kth moments of live and dead polymers are defined as $\lambda_{Pk} \equiv \sum_{n=1}^{\infty} n^k[P_n]$ and $\lambda_{Mk} \equiv \sum_{n=1}^{\infty} n^k[M_n]$, respectively. [P] is the total live polymer concentration and $[P] = \lambda_{P0}$.

Number-average and weight-average molecular weights are calculated using the following equations:

$$\overline{M}_n = \frac{\lambda_{P1} + \lambda_{M1}}{\lambda_{P0} + \lambda_{M0}}(mw)_{sty} \approx \frac{\lambda_{M1}}{\lambda_{M0}}(mw)_{sty} \tag{17}$$

$$\overline{M}_w = \frac{\lambda_{P2} + \lambda_{M2}}{\lambda_{P1} + \lambda_{M1}}(mw)_{sty} \approx \frac{\lambda_{M2}}{\lambda_{M1}}(mw)_{sty} \tag{18}$$

where $(mw)_{sty}$ represents the molecular weight of styrene. Notice that in Eqs. (17) and (18), the contributions of live polymers to overall molecular weight averages are ignored because the concentrations of live polymers are far smaller than the concentration of dead polymers. Also, in the above kinetic model, we assumed that the catalyst is a single site catalyst. Later in our discussion, we shall examine the validity of this assumption.

In the mathematical derivation of the foregoing polymerization model, the monomer concentration $[M]_s$ represents the monomer concentration at the catalytic sites in the solid phase. In a heterogeneous reaction system such as considered in this work, it is possible that the monomer concentration in the bulk liquid phase ($[M]_b$) may not be same as that in the solid phase. Recall that in Fig. 2, we have observed the deviation of the polymerization rate from the first-order dependence on the bulk phase monomer concentration. The non-linear rate dependence of polymerization rate on monomer concentration is often observed in other catalyzed polymerization processes such as ethylene slurry polymerization with metallocene catalysts [12]. But the polymerization rate patterns observed in our system and liquid slurry ethylene polymerization systems reported in the literature are different. For example, in ethylene polymerization, reversible complex formation occurs between an active site and a monomer molecule, leading to the transition from the second-order kinetics to the first-order kinetics as monomer concentration is increased. In our polymerization, however, the polymerization shows the first-order kinetics ($R_p \propto [M]$) at low monomer concentrations ($[M]_{b0} < 2.0$ mol/L) but the polymerization rate deviates from the first-order kinetics as monomer concentration is increased (e.g., $[M]_{b0} > 2.0$ mol/L). We had tried a power-law kinetic model to fit the data (e.g., $R_p = k_p[M]_b^{\alpha}[C^*]$), but the power-law model was inadequate to fit the data shown in Fig. 1.

To analyze the non-linear rate dependence on monomer concentration, we propose that the monomer concentration in the solid phase (liquid–swollen polymer phase) is non-linearly related to the monomer concentration in the bulk liquid phase. In ethylene or propylene polymerization in liquid slurry phase with transition metal catalysts, monomer partition occurs between the bulk liquid phase and the solid polymer particle phase [13]. In bulk free radical polymerization of vinyl chloride similar particle precipitation phenomena occur [14,15]. For example, according to Patel et al. [16] who performed sorption experiments with poly(vinyl chloride) (PVC) particles and vinyl chloride in water, the monomer concentrations in the bulk liquid phase and in

the solid phase are non-linearly related. They fitted the experimental monomer sorption data with a Langmuir isotherm type monomer partition equation. In our work, we employ a similar empirical correlation for the partition of styrene between the bulk liquid phase ($[M]_b$) and the solid phase ($[M]_s$):

$$[M]_s = \frac{K_1[M]_b}{1 + K_2[M]_b} \tag{19}$$

According to Eq. (19), the monomer concentration in the solid phase increases linearly with the bulk phase concentration at low $[M]_b$ but it approaches the saturation value (i.e., $[M]_{sat} = K_1/K_2$ at high $[M]_b$. If we adopt the form given in Eq. (19), the polymerization rate is expressed as:

$$R_p = k_p[M]_s[C^*] = \frac{k_p K_1[M]_b}{1 + K_2[M]_b}[C^*] \equiv \frac{k'_p[M]_b}{1 + K_2[M]_b}[C^*] \tag{20}$$

where $k'_p \triangleq k_p K_1$ represents the effective propagation rate constant. We can rearrange Eq. (20) as follows:

$$\frac{[C^*]_0}{R_{p0}} = \frac{K_2}{k'_p} + \frac{1}{k'_p}\frac{1}{[M]_{b0}} \tag{21}$$

Fig. 4 shows the test of Eq. (21) applied to our polymerization rate data. Notice that the experimental data are well fitted by Eq. (21). The kinetic parameter values obtained from Fig. 4 are: $k'_p = 8.15 \times 10^3$ L/mol h, $K_2 = 0.47$ L/mol. Unfortunately, the value of K_1 cannot be obtained separately because it is not possible to directly measure the monomer concentration in the solid phase.

Another factor that can contribute to the decrease in the polymerization rate is the catalyst deactivation. Although the site deactivation mechanisms and kinetics are not well understood for most of the transition metal catalyzed olefin polymerization processes, first-order deactivation kinetics has been generally well accepted. If we assume the first-order deactivation kinetics, the polymerization rate equation can be expressed as follows:

$$R_p = \frac{k'_p[M]_b}{1 + K_2[M]_b}[C^*]_0 e^{-k_d t} \tag{22}$$

The deactivation rate constant was estimated using Gauss–Newton method based on non-linear least squares regression (*nlinfit* function in MATLAB® package, The MathWorks, Inc., Ver. 6.5) and the polymerization rate data shown in Fig. 1(b). The deactivation rate constant value obtained at 70 °C is $k_d = 1.67$/h.

We used the modified polymerization rate model (Eq. (22)) to calculate the polymer yield and the results are shown in Fig. 1(a) and (b). The model simulation results (lines) show that the proposed polymerization rate model yields a good fit to the experimental data (symbols). The predictions of initial polymerization rates at different monomer concentrations are also shown in Fig. 1(b). The model tends to under predict the polymerization rate at $t = 120$ min.

3.2. Physical changes during polymerization

We have mentioned that a reaction mixture undergoes a series of physical changes during the sPS polymerization. Fig. 5 shows a schematic illustration of the physical changes of reaction mixture we have observed with silica-supported metallocene catalyst.

Fig. 6 illustrates the physical changes of the reaction mixture at different solid contents during the polymerization. At very low TSC, the reaction mixture is a clear liquid with no visible particle precipitation. As TSC increases to about 1%, precipitation of polymer particles becomes visible and the reaction mixture becomes turbid. Initially, the polymer precipitates are not hard and discrete particles. They begin to agglomerate to form soft or very low density aggregates (Fig. 6(a)). These aggregates become larger as conversion increases and they look like 'marsh-mallows' (Fig. 6(b)). As TSC increases further, the collision of these agglomerates becomes more frequent and they become smaller and dense (Fig. 6(c)). Then, these solid particles imbibe the liquid and the reaction mixture becomes a wet cake-like material (Fig. 6(d)). At this stage, a separate liquid phase is no longer visible and polymer particles are wetted by the liquid (solvent and monomer). When the initial styrene concentration was high (i.e., small solvent volume fraction), the wet cake eventually became dry particles (Fig. 6(e) and (f)). Indeed, when we opened the reactor after experiment, the reactor was filled with relatively dry particles with no liquid phase (diluent and styrene) (Fig. 6(f)). It was a quite interesting series of physical changes.

To measure the amount of liquid imbibed in sPS, we carried out absorption experiments with sPS particles. Dried sPS particles were charged into glass vials and a styrene–solvent mixture was doled out to each vial. The glass vial was immersed in a constant temperature bath. After a vial was removed from the bath at a predetermined sampling time, the solid–liquid mixture was filtered and the weight of the liquid swollen

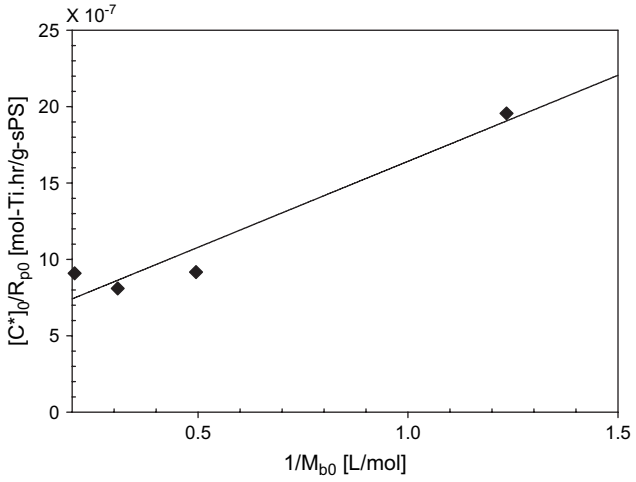

Fig. 4. Test of Eq. (21).

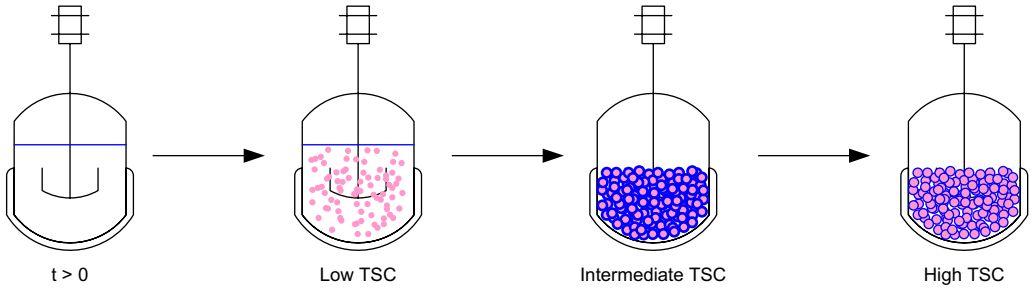

Fig. 5. Schematic illustration of the sPS slurry polymerization process.

polymer particles was measured. Fig. 7 shows the amount of absorbed styrene–solvent mixture in sPS solid phase. The amount of liquid absorbed in 1 g of sPS polymer (Φ) is fitted by the following equation:

$$\Phi = 6.2 + 0.18[\mathrm{M}]_{\mathrm{b}} \tag{23}$$

Using Eq. (23), we can calculate the volumes of bulk liquid and solid phases with reaction time. The total slurry volume (V_{slurry}) is represented by:

$$V_{\mathrm{slurry}} = \frac{W_{\mathrm{M}}}{\rho_{\mathrm{M}}} + \frac{W_{\mathrm{D}}}{\rho_{\mathrm{D}}} + \frac{W_{\mathrm{sPS}}}{\rho_{\mathrm{sPS}}} \tag{24.1}$$

where ρ_{M}, ρ_{D}, and ρ_{sPS} are the densities of monomer, diluent and sPS, respectively. The liquid phase volume is calculated by:

$$V_{\mathrm{L}} = V_{\mathrm{slurry}} - \Phi W_{\mathrm{sPS}} - \frac{W_{\mathrm{sPS}}}{\rho_{\mathrm{sPS}}} \tag{24.2}$$

Then, the change in the slurry phase volume with reaction time is represented as:

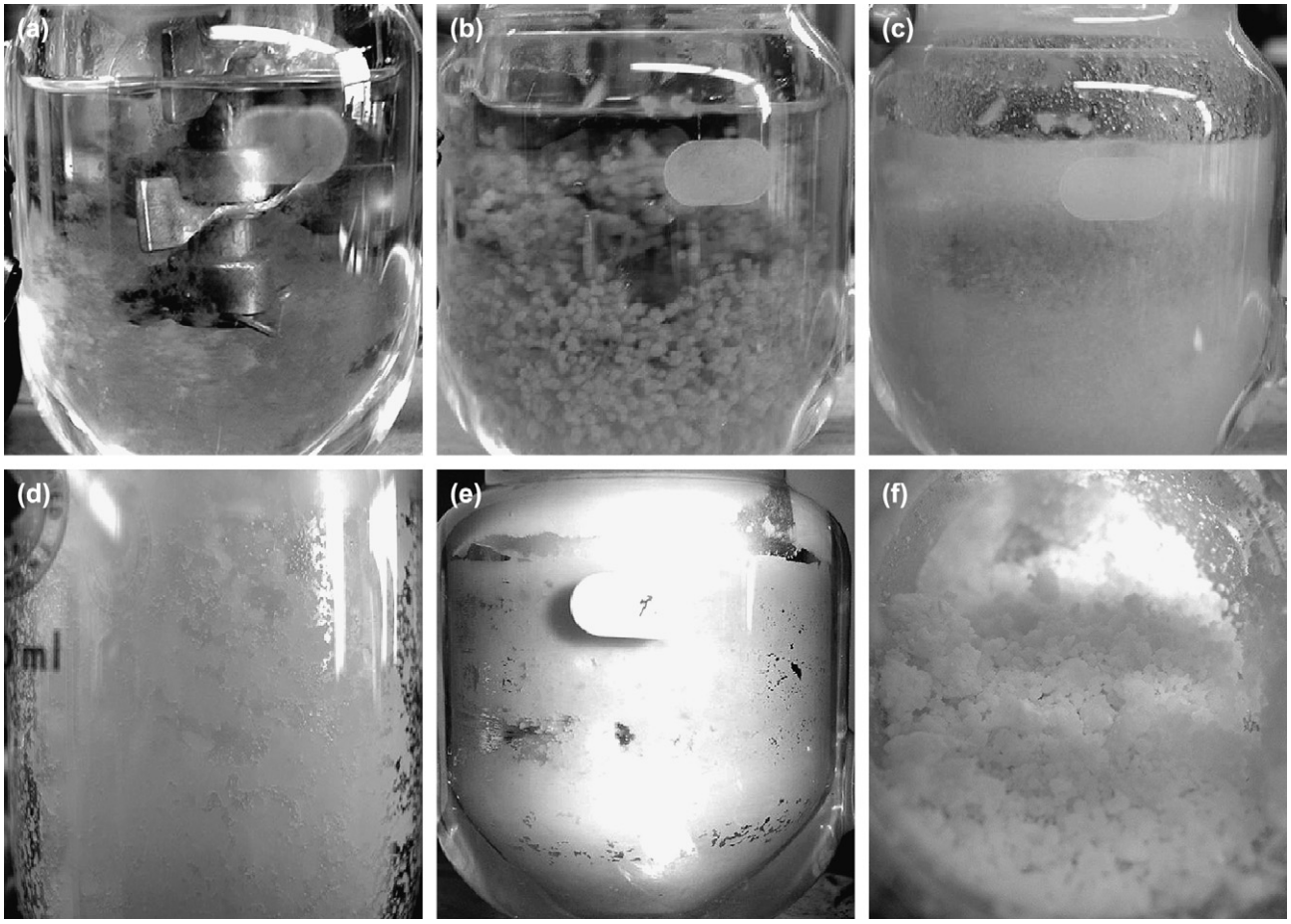

Fig. 6. The photographs of physical phases of a polymerization mixture (a) TSC = 0.8 w/w%; (b) TSC = 3.6 w/w%; (c) TSC = 8.71 w/w%; (d) TSC = 12.4 w/w%; (e) TSC = 20.5 w/w%; (f) TSC = 19.1 w/w%.

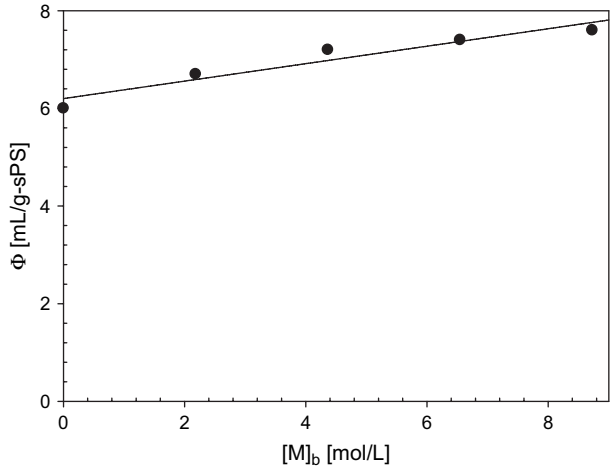

Fig. 7. The amount of styrene–heptane mixture absorbed in sPS polymer ($T = 70$ °C; ●, data; line – regression).

$$\frac{dV_{slurry}}{dt} = \frac{1}{\rho_M}\frac{dW_M}{dt} + \frac{1}{\rho_{sPS}}\frac{dW_{sPS}}{dt} = \left(\frac{1}{\rho_{sPS}} - \frac{1}{\rho_M}\right)V_{slurry}R_p \quad (25)$$

Eq. (25) was solved with the kinetic model equations. Fig. 8(a) and (b) shows the calculated volume fractions of liquid phase and the total solid content for different initial styrene concentrations. Fig. 8(a) shows that at high initial monomer concentrations, a separate liquid phase disappears after about 35 min ($[M]_{b0} = 4.86$ mol/L) or 50 min ($[M]_{b0} = 3.24$ mol/L) at which the total solid contents are 15.7 wt.% and 16.5 wt.%, respectively (Fig. 8(b)). The results in Fig. 8(a) match the visual observations as shown in Fig. 6. Fig. 8(a) also indicates that slurry phase is always maintained at low initial monomer concentrations (e.g., $[M]_{b0} < 2.02$ mol/L) because the amount of sPS particles produced is not sufficient to absorb the whole liquid.

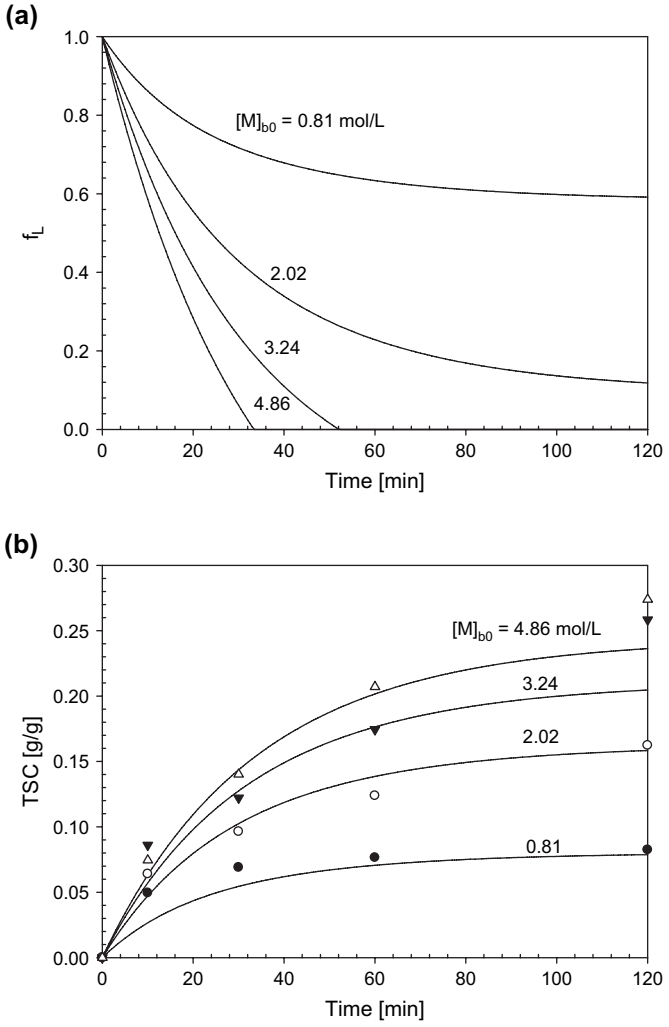

Fig. 8. (a) The volume fraction of liquid phase vs. reaction time; (b) the TSC profiles vs. reaction time (symbols – data (●, 0.81 mol/L; ○, 2.02 mol/L; ▼, 3.24 mol/L; △, 4.86 mol/L), lines – model).

3.3. Molecular weight distribution analysis

We also investigated the effect of reaction time and monomer concentration on the polymer molecular weight and molecular weight distribution. Fig. 9 (symbols) shows the experimental data of molecular weight averages with reaction time for the initial monomer concentration of 3.24 mol/L. As commonly observed in many other addition polymerization processes, both the number-average ($\overline{M}_n$) and the weight-average ($\overline{M}_w$) molecular weight values increase rapidly in short reaction time at the beginning of polymerization and then slightly decrease with time. Fig. 10 shows the effect of monomer concentration on $\overline{M}_n$ and $\overline{M}_w$. In this graph, we used the effective bulk monomer concentration calculated from the polymer yield. The molecular weight average values are those obtained after 30 min of reaction.

It is interesting to notice that the molecular weight increases with an increase in monomer concentration. In olefin polymerization processes with either Ziegler–Natta or metallocene catalysts, polymer molecular weight is not influenced by the bulk phase monomer concentration when the chain transfer to monomer is the dominant mode of chain transfer reaction (i.e., $\overline{X}_n \approx k_p/k_{tM}$; Eq. (26)). The dependence of sPS molecular weight on styrene concentration suggests that other chain transfer reactions such as β-hydrogen elimination are also important.

To calculate polymer molecular weight averages and molecular weight distribution, several kinetic parameters need to be estimated. They are the chain propagation rate constant (k_p), the monomer chain transfer rate constant (k_{tM}), and the β-hydrogen elimination rate constant ($k_{t\beta}$). To obtain the initial estimates of these rate constants, we first assume that the catalyst is a single site catalyst and catalyst deactivation has little effect on the polymer molecular weight properties. Then, the instantaneous number-average degree of polymerization can be represented by the following equation [6,7]:

$$\overline{X}_n = \frac{R_p}{R_t + R_d} = \frac{k_p[M]_s[P]}{k_{tM}[M]_s[P] + k_{t\beta}[P] + k_d[P]} \quad (26)$$

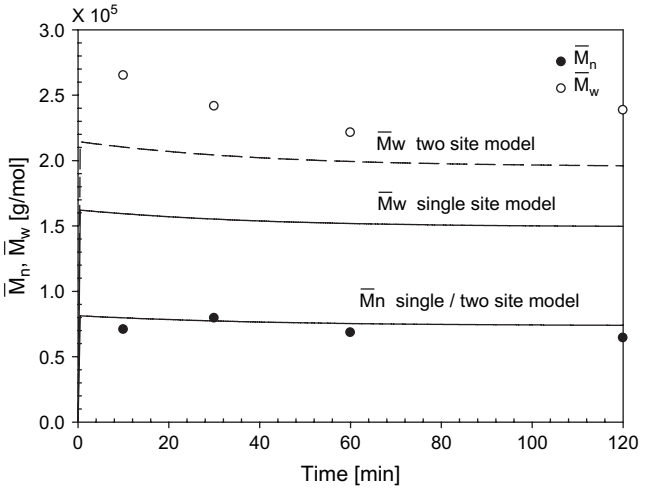

Fig. 9. SPS molecular weight profiles for $[M]_{b0} = 3.24$ mol/L (symbols – experimental data, lines – model: dashed lines – $\overline{M}_w$).

where R_p is the chain propagation rate, R_t is the total chain transfer rates, and R_d is the site deactivation rate. [P] represents the total active site concentration (i.e., $[P] = [C^*] + \sum_{n=1}^{\infty}[P_n]$). Eq. (26) can be rearranged to:

$$\frac{1}{\overline{X}_n} = \frac{k_{tM}}{k_p} + \frac{k_{t\beta} + k_d}{k_p}\frac{1}{[M]_s} = \frac{k'_{tM}}{k'_p} + \frac{K_2(k_{t\beta} + k_d)}{k'_p} + \frac{k_{t\beta} + k_d}{k'_p}\frac{1}{[M]_b} \tag{27}$$

where $k'_{tM} \triangleq k_{tM}K_1$. It should be pointed out that the molecular weight averages measured experimentally are cumulative molecular weight values at specific sampling times. In sPS polymerization and also in most of α-olefin polymerizations with transition metal catalysts, number-average molecular weight ($\overline{M}_n$) increases almost instantly to a large value with a very slow decrease with time (e.g., Fig. 9). So, using Eqs. (26) and (27), we assume that the $\overline{X}_n$ values are approximately equal to the cumulative $\overline{X}_n$ values. Indeed, this approximation has been used in the kinetic analysis of polymer molecular weight distribution in most of the non-living addition polymerization processes (e.g., free radical and coordination polymerizations) [17,18].

Eq. (27) indicates that by plotting $1/\overline{X}_n$ against $1/[M]_b$, we can estimate the rate constant values. Fig. 11 shows the test of Eq. (27). Although we used a single site catalyst model, Fig. 11 shows that the linear fit is quite satisfactory. Table 2 shows the rate parameter values obtained from Fig. 11. Recall that the effective propagation rate constant (k'_p) and the monomer partition constant (K_2) were determined from the polymerization rate analysis. The estimated chain transfer rate constants also indicate that both monomer chain transfer and β-hydrogen elimination reactions strongly affect the polymer molecular weight.

With these kinetic rate constants, we solved the molecular weight moment equations to calculate the weight-average molecular weight. The solid lines in Figs 9 and 10 are the resulting single site model calculations. Here, we observe that the predicted number-average molecular weight values are in very good agreement with experimental data but the model calculated weight-average molecular weights are lower than the experimentally measured. In a single site model, the polymer chain length distribution follows Schulz–Flory distribution which gives rise to the predicted polydispersity ($\overline{M}_w/\overline{M}_n$) of 2.0. As shown in Table 1 and Figs. 9 and 10, the sPS polydispersity values are always larger than 2.0, suggesting that catalytic site heterogeneity may exist in the silica-supported catalyst used in our study. It is also possible that metallocene catalyst might have leached out from the solid phase during the polymerization and initiate homogeneous polymerization in the bulk liquid phase, contributing to the broadening of MWD [19,20].

Although many homogeneous metallocene catalysts are known to have a uniform type of catalyst site and hence called as single site catalysts, there are many reports that heterogenized metallocene catalysts often result in broad polymer molecular weight distributions, most notably in α-olefin and

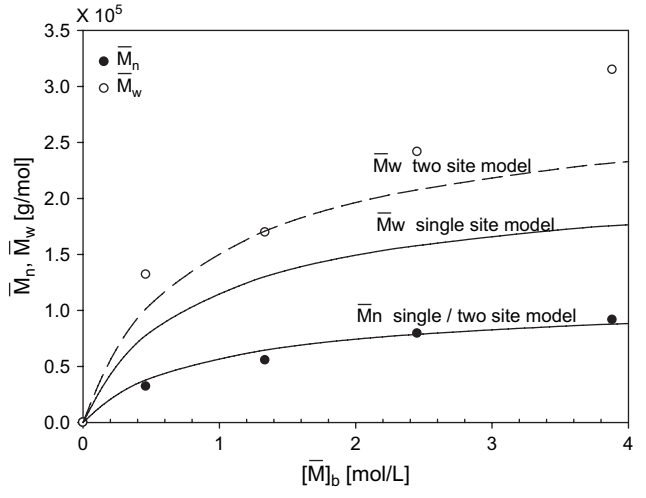

Fig. 10. Polymer molecular weights at different monomer concentrations (reaction time = 30 min; symbols – data, lines – model).

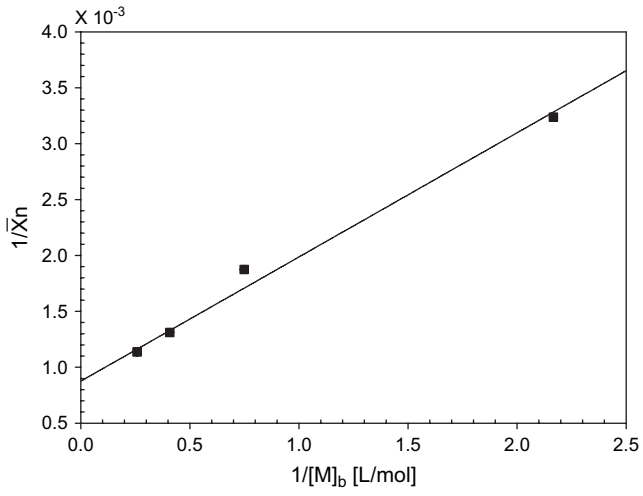

Fig. 11. Plot of Eq. (27) to determine rate constants.

Table 2
The reaction rate constants (single site)

K'_p [L/mol h]	K_2 [L/mol]	k_d [1/h]	$k_{t\beta}$ [1/h]	K'_{tM} [L/mol h]
8150	0.47	1.67	7.81	3.11

styrene polymerizations. For example, Frauenrath et al. [21,22] reported that deviations from the single site behavior of metallocene catalysts occur in 1-hexene polymerization with zirconocene/MAO catalyst system. Kou et al. [23] proposed two active sites model of homopolymerization of ethylene with silica-supported metallocene catalysts. Their model is based on the reactivity of several surface functional groups of a silica support and metallocene catalysts. Deviations from single site catalytic behavior of metallocene catalysts have also been observed in previous sPS polymerization studies (see Schellenberg and Tomotsu's review paper [4]). It is now generally accepted that the broadening of MWD in heterogeneously catalyzed olefin polymerization is caused primarily by the presence of multiple active sites of different catalytic activity and selectivity. Monomer diffusion resistance and catalyst leaching effect can also affect the MWD broadening but their effects are not as strong as that of catalytic site heterogeneity.

3.4. Two-site model

We shall modify the single site model by considering the site heterogeneity in the silica-supported $Cp^*Ti(OCH_3)_3$/MAO catalyst as a main cause of MWD broadening. When a metallocene catalyst is supported onto a silica by forming a complex with MAO that is already anchored onto a silica surface, it is likely that the activity of the catalyst will be influenced by the heterogeneity of the silica–MAO complex, causing the site heterogeneity [24]. A silica surface is known to have different types of surface structures represented by single (isolated) silanols, silanediols (geminal), H-bonded vicinal silanols (vicinals), etc. [25]. The concentrations of surface hydroxyl groups that may affect the catalyst reactivity are dependent upon the calcination temperature [26]. For example, when a silica gel is calcined at 250–300 °C or above, geminal groups exist only in limited amount and single silanol and vicinal groups exist almost 50% each [27,28]. Fig. 12 illustrates the possible surface structures of silica gel and the complexes of MAO and surface groups of the silica. If the main catalyst component is supported onto the surface hydroxyl groups of different structures, it is quite possible that each catalyst site can exhibit different polymerization activity.

It should be pointed out that although the site heterogeneity of a silica surface may be present, it will be a challenging task to identify the number of different catalytic site types and their functions as active catalysts. One of the pragmatic methods used by many researchers is the MWD deconvolution technique where experimentally measured broad MWD of heterogeneously polymerized polyolefins is matched with multiple Schulz–Flory distribution curves [29–31]. In this technique, it is assumed that the polymer chain length distribution at each type of catalyst site follows Schulz–Flory distribution. By adjusting the kinetic constants and the mass fraction of each site, one can match the experimentally observed MWD

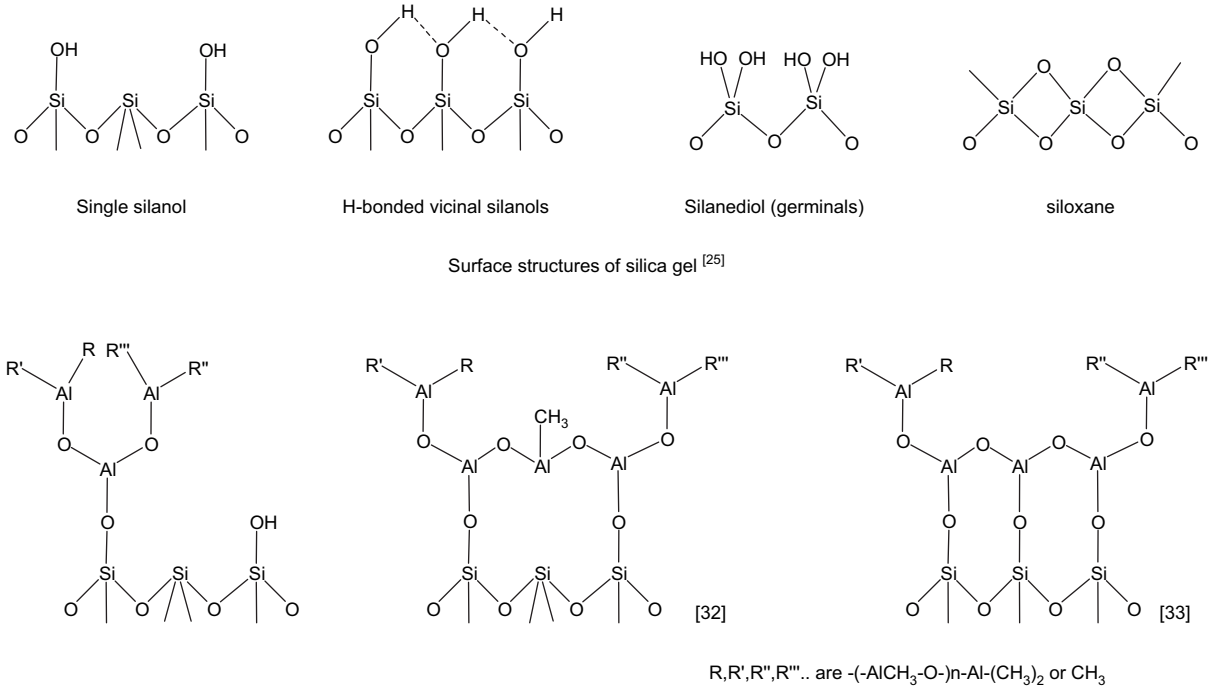

Fig. 12. The surface groups of silica gel and the complexes of MAO and the surface groups of silica [25,32,33].

with the model. In practice, it is difficult to determine the unique set of relevant kinetic parameters for each site.

In our model, we shall employ a two-site model as an approximation of a multi-site model to calculate the MWD of sPS. We assume that the catalytic sites have same polymerization activity (propagation activity) but they differ in their chain transfer capabilities. The two-site model is the simplest of the multi-site model and its main advantage is that the number of adjustable parameters is minimal. Certainly if the two-site model fails to fit the experimentally measured polymer molecular weight distribution, more active sites can be added into a model. Of course, then, there is a burden that increased number of parameters that needs to be estimated by numerical means (parameter optimization methods). In our analysis, we fix the propagation and deactivation rate constants to minimize the arbitrariness in fitting the MWD.

For a catalyst of multiple active sites, the weight fraction of the polymer of chain length x produced by the active site i ($W_i(x)$) is given by the following Schulz–Flory distribution function [29–31]:

$$W_i(x) = \tau_i^2 x \exp(-\tau_i x) \tag{28}$$

where the parameter τ_i is defined as follows:

$$\tau_i = \frac{R_{t,i} + R_{d,i}}{R_{p,i}} \tag{29}$$

Then, the weight chain length distribution of sPS is calculated by the following equation:

$$X_w = \sum_i \phi_i x W_i(x) \tag{30}$$

where ϕ_i is the weight fraction of active site i. With the propagation and deactivation rate constants fixed for each site, τ_i is changed by adjusting the termination rate constants ($k_{t\beta}$, and k'_{tM}) and the weight fraction of each active site ϕ_i. The overall termination rate constant determined from Fig. 9 is also kept constant. Then, only three parameters – $k_{t\beta,1}$, $k'_{tM,1}$ and ϕ_1 – are needed to be estimated. Using the non-linear least squares regression technique in MATLAB®, these three parameters were estimated. $k_{t\beta,2}$, $k'_{tM,2}$ and ϕ_2 are calculated as:

$$\phi_2 = 1 - \phi_1 \tag{31}$$

$$k_{t\beta} = \phi_1 k_{t\beta,1} + \phi_2 k_{t\beta,2} \tag{32}$$

$$k'_{tM} = \phi_1 k'_{tM,1} + \phi_2 k'_{tM,2} \tag{33}$$

The kinetic parameters for the two-site model were estimated using the experimentally measured MWD data shown in Figs. 13 and 14 and Table 3 shows the parameter values determined using the optimal parameter estimation technique. Fig. 13 shows the comparison of experimental MWD data (symbols) and the two-site model predictions (long dashed lines). The two small curves marked by dashed lines are the MWD for each of the two single sites used in the two-site model. Also shown in Fig. 13 is the MWD curve by the single site model

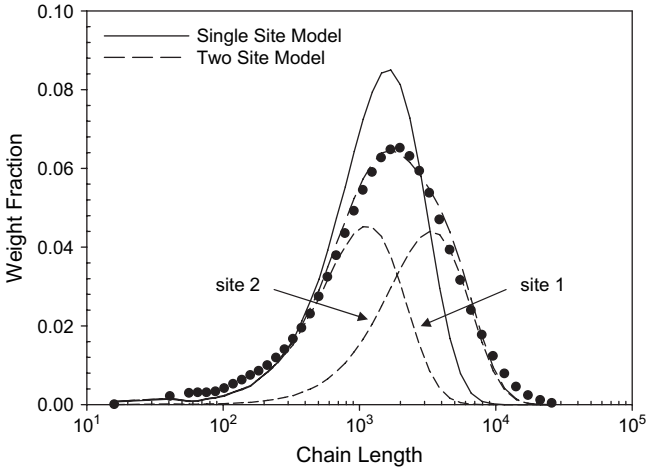

Fig. 13. Experimental and model-predicted molecular weight distribution curves for $[M]_{b0} = 3.24$ mol/L, $t = 30$ min (symbols – data, lines – model predictions).

(solid line). Notice that the single site model is inadequate in predicting the MWD whereas the two-site model yields a significantly improved prediction of MWD. With the model parameter values shown in Table 3, we also calculated the MWD for other polymerization experiments with different initial monomer concentrations. The model predictions and the experimental MWD curves are shown in Fig. 14. Some discrepancies between the data and the model predictions are clearly present but the two-site model provides a reasonable quality prediction of MWD for each case without additional adjustment of parameter values. Certainly, the model fidelity can be improved by adding third active site into the model but as mentioned earlier, it will be very difficult to find unique set of parameters without uncertainty unless additional data of site characteristics are available.

Finally, we would like to make a remark on the under predicted polymerization rates by the kinetic model at

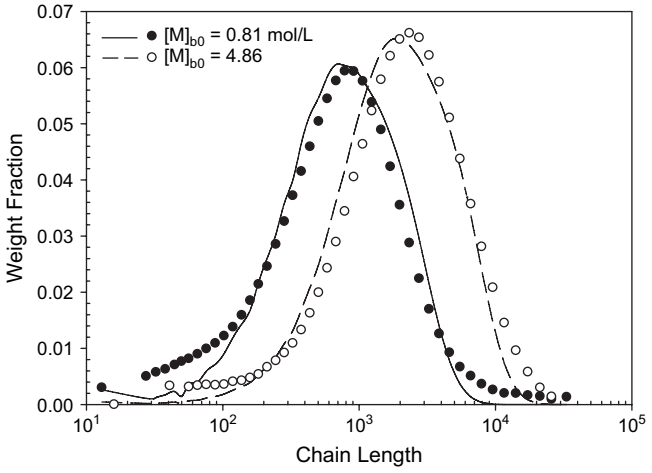

Fig. 14. Experimental and model-predicted molecular weight distribution curves at different initial monomer concentrations ($t = 30$ min, symbols – data, lines – model predictions).

Table 3
Two-site model parameters

$K'_{p,1}$ [L/mol h]	$K'_{p,2}$ [L/mol h]	k_d [1/h]	$k_{t\beta,1}$ [1/h]	$k_{t\beta,2}$ [1/h]	$k'_{tM,1}$ [L/mol h]	$k'_{tM,2}$ [L/mol h]	K_2 [L/mol]	ϕ_1 [−]
8150	8150	1.67	10.98	3.94	5.10	0.68	0.47	0.55

$t = 120$ min shown earlier in Fig. 1(b) (lines). Recall that the polymerization rate was predicted using the single site model. In our two-site modeling, we assumed that the two different sites are represented by the same propagation rate constant (k_p) and the deactivation rate constant (k_d). Therefore, both the single site model and the two-site model yield the same polymerization rate. However, it is certainly possible that each site can also have different propagation and deactivation rate constants, making one of the two sites to deactivate faster than the other, affecting the overall polymerization rate. Practically, however, it will be very difficult, if not impossible, to discern the differences in the polymerization activities of the two different catalytic sites when the overall polymerization rate and molecular weight data are the only available process data that can be measured. Finally, we would like to comment that although the predicted polymerization rates at $t = 120$ min in Fig. 1(b) are lower than the experimentally measured, these under predicted polymerization rates have little effect on the polymer yield as shown in Fig. 1(a). It is because the amount of polymer produced after 60 min is very small.

4. Conclusions

This paper reports new experimental and theoretical modeling analysis of the syndiospecific polymerization of styrene over silica-supported Cp*Ti$(OCH_3)_3$/MAO catalyst. The use of silica-supported catalyst in a liquid slurry polymerization has been very effective in obtaining non-agglomerated sPS particles. It has been observed that sPS polymerization rate is non-linearly dependent on the bulk phase monomer concentration. This is attributed to the partition of monomer between the solid and the liquid phases. We incorporated the monomer partition effect into our kinetic model and obtained a very good fit of the experimental data. The estimated partition parameter values suggest that the monomer concentration in the solid phase is lower than the bulk liquid phase concentration. Another important point in a liquid slurry polymerization of styrene is that an sPS slurry undergoes a series of physical changes during the polymerization. The use of silica-supported metallocene catalyst was quite effective in preventing the formation of gels in the reactor. We observed that a separate liquid phase can completely disappear at about 15–20 wt.% of solid phase when high monomer concentrations are used. It is because unreacted monomer and diluent are absorbed by the solid polymer phase.

In general, very narrow MWD is obtained when a homogeneous metallocene catalyst is used. In our experiments with a heterogeneous silica-supported Cp*Ti$(OCH_3)_3$/MAO catalyst, we observed that sPS molecular weight distributions were broad (i.e., $\overline{M}_w/\overline{M}_n > 20$), indicating a significant departure from the single site polymerization kinetics. We modeled the MWD distribution broadening by employing a two-site kinetic model. Using the polymerization rate and MWD data, we estimated the relevant model parameters. The two-site model provided improved predictions of the molecular weight distribution, clearly suggesting the presence of multiple active sites in the silica-supported metallocene catalyst used in our study.

Acknowledgements

We are indebted to a financial support by LG Chemical Company for this work. Jason Gordon (currently at Columbia University, New York, NY) contributed to this work through sorption experiments. We also thank Dr. Mooho Hong at LG Chem, Ltd. Research Park for the high temperature GPC analysis of sPS samples.

References

[1] Schellenberg J, Leder HJ. Adv Polym Technol 2006;25(3):141–51.
[2] Ishihara N, Seimiya T, Kuramoto M, Uoi M. Macromolecules 1986;19(9):2464–5.
[3] Ishihara N, Kuramoto M, Uoi M. Macromolecules 1988;21(12):3356–60.
[4] Schellenberg J, Tomotsu N. Prog Polym Sci 2002;27(9):1925–82.
[5] Oliva L, Pellecchia C, Cinquina P, Zambelli A. Macromolecules 1989;22(4):1642–5.
[6] Grassi A, Lamberti C, Zambelli A, Mingozzi I. Macromolecules 1997;30(7):1884–9.
[7] Fan R, Li BG, Cao K, Zhou WL, Shen ZG, Ye M. J Appl Polym Sci 2002;85(13):2635–43.
[8] Choi KY, Chung JS, Woo BG, Hong MH. J Appl Polym Sci 2003;88(8):2132–7.
[9] Chung JS, Woo BG, Choi KY. Macromol Symp 2004;206:375–82.
[10] Lee HW, Chung JS, Choi KY. Polymer 2005;46(14):5032–9.
[11] Po R, Cardi N. Prog Polym Sci 1996;21(1):47–88.
[12] Bergstra MF, Weickert G. Macromol Mater Eng 2005;290(6):610–20.
[13] Hutchinson RA, Ray WH. J Appl Polym Sci 1990;41(1–2):51–81.
[14] Xie TY, Hamielec AE, Wood PE, Woods DR. Polymer 1991;32(3):537–57.
[15] Xie TY, Hamielec AE, Wood PE, Woods DR. Polymer 1991;32(6):1098–111.
[16] Patel CB, Grandin RE, Gupta R, Phillips EM, Reynolds CE, Chan RKS. Polym J 1979;11(1):43–51.
[17] Young RJ, Lovell PA. Introduction to polymers. 2nd ed. London; New York: Chapman & Hall; 1991.
[18] Odian G. Principles of polymerization. 4th ed. New York; Chichester: Wiley; 2004.
[19] Kaminsky W, Winkelbach H. Top Catal 1999;7(1–4):61–7.
[20] Novokshonova L, Kovaleva N, Meshkova I, Ushakova T, Krasheninnikov V, Ladygina T, et al. Macromol Symp 2004;213:147–55.
[21] Frauenrath H, Keul H, Hocker H. Macromol Chem Phys 2001;202(18):3543–50.
[22] Frauenrath H, Keul H, Hocker H. Macromol Chem Phys 2001;202(18):3551–9.
[23] Kou B, McAuley KB, Hsu CC, Bacon DW, Yao KZ. Ind Eng Chem Res 2005;44(8):2428–42.
[24] Ciardelli F, Altomare A, Michelotti M. Catal Today 1998;41(1–3):149–57.
[25] Ullmann's encyclopedia of industrial chemistry. 1st ed. Wiley; 1993.
[26] van Grieken R, Calleja G, Serrano D, Martos C, Melgares A, Suarez I. Polym React Eng 2003;11(1):17–32.

[27] Haukka S, Lakomaa EL, Root A. J Phys Chem 1993;97(19):5085–94.
[28] Zhuravlev LT. Colloids Surf A 2000;173(1–3):1–38.
[29] Soares JBP, Hamielec AE. Polymer 1995;36(11):2257–63.
[30] Soares JBP, Kim JD, Rempel GL. Ind Eng Chem Res 1997;36(4): 1144–50.
[31] Tannous K, Soares JBP. Macromol Chem Phys 2002;203(13):1895–905.
[32] Juan A, Damiani D, Pistonesi C, Garcia A. Macromol Theory Simul 2001;10(5):485–90.
[33] Van Grieken R, Carrero A, Suarez I, Paredes B. Eur Polym J 2007;43(4): 1267–77.